SCIENTIFIC REPORTS

OPEN

Received: 4 July 2017
Accepted: 18 December 2017
Published online: 10 January 2018

Sweep Dynamics (SD) plots: Computational identification of selective sweeps to monitor the adaptation of influenza A viruses

Thorsten R. Klingen[1], Susanne Reimering[1], Jens Loers[1], Kyra Mooren[1], Frank Klawonn[2,3], Thomas Krey[4,5], Gülsah Gabriel[6,7] & Alice C. McHardy[1,5]

Monitoring changes in influenza A virus genomes is crucial to understand its rapid evolution and adaptation to changing conditions e.g. establishment within novel host species. Selective sweeps represent a rapid mode of adaptation and are typically observed in human influenza A viruses. We describe Sweep Dynamics (SD) plots, a computational method combining phylogenetic algorithms with statistical techniques to characterize the molecular adaptation of rapidly evolving viruses from longitudinal sequence data. SD plots facilitate the identification of selective sweeps, the time periods in which these occurred and associated changes providing a selective advantage to the virus. We studied the past genome-wide adaptation of the 2009 pandemic H1N1 influenza A (pH1N1) and seasonal H3N2 influenza A (sH3N2) viruses. The pH1N1 influenza virus showed simultaneous amino acid changes in various proteins, particularly in seasons of high pH1N1 activity. Partially, these changes resulted in functional alterations facilitating sustained human-to-human transmission. In the evolution of sH3N2 influenza viruses, we detected changes characterizing vaccine strains, which were occasionally revealed in selective sweeps one season prior to the WHO recommendation. Taken together, SD plots allow monitoring and characterizing the adaptive evolution of influenza A viruses by identifying selective sweeps and their associated signatures.

Influenza A viruses are rapidly evolving pathogens causing respiratory infections with high morbidity and mortality in the human population[1]. Annual influenza epidemics result in 3 to 5 million reported infections and up to 250,000–500,000 cases of death[1]. Currently, the viral subtypes sH3N2 and pH1N1 are circulating in the human population. The H3N2 virus was introduced into the human population in 1968 and is endemic ever since. The swine-origin H1N1 subtype emerged in the 2009 influenza pandemic and was subsequently referred to as the 2009 pH1N1 virus. It replaced the formerly circulating seasonal H1N1 subtype[2,3]. The negative-sense RNA genome consists of eight segments that encode for 14 viral proteins[4]. A constant arms-race between the human immune system and the virus results in continuous adaptation of the viral genome. These changes facilitate the virus to escape the host's immune response elicited through vaccination or previous influenza infections[5]. Alterations in the major glycoproteins – hemagglutinin (HA) and neuraminidase (NA) – and genomic reassortment that change the viral antigenicity are defined as antigenic drift and result in re-occurring epidemics of seasonal influenza viruses[6]. Continuous antigenic changes of circulating strains require a re-evaluation of antigenically predominant strains by the WHO twice a year at the end of each season, leading to a recommendation for the vaccine composition for the following year[7–9]. The establishment of an antigenically new virus strain into an immunologically naive human population causes pandemics, mostly due to alterations in the receptor binding protein HA[10].

[1]Department for Computational Biology of Infection Research1, Helmholtz Center for Infection Research, Braunschweig, Germany. [2]Biostatistics Group, Helmholtz Center for Infection Research, Braunschweig, Germany. [3]Department of Computer Science, Ostfalia University of Applied Sciences, Wolfenbüttel, Germany. [4]Institute of Virology, Hannover Medical School, Hannover, Germany. [5]German Center for Infection Research (DZIF), Braunschweig, Germany. [6]Viral Zoonoses and Adaptation, Heinrich Pette Institute, Leibniz Institute for Experimental Virology, Hamburg, Germany. [7]University of Lübeck, Lübeck, Germany. Thorsten R. Klingen and Susanne Reimering contributed equally to this work. Correspondence and requests for materials should be addressed to A.C.M. (email: Alice.McHardy@helmholtz-hzi.de)

Measuring the impact of natural selection plays a crucial role in molecular evolution, as it determines the genomic constitution and diversity of a population[11]. Directional evolutionary processes boost the fitness of individuals by introducing advantageous amino acids. The respective alleles rise in frequency in the viral population, consequentially reducing variation. This process is called a 'selective sweep'[12]. Hereafter, we use the term 'sweep-related change' when referring to an amino acid exchange rising in frequency due to a selective sweep. Due to linkage within genomic segments, the advantageous amino acid exchange promoting the sweep and other changes in close genomic proximity jointly rise in frequency, leading to an increase of linkage disequilibrium (i.e. nonrandom associations between genomic regions). Thus, selective sweeps are of profound interest since they represent a rapid shift of the whole genotype carrying the selected amino acid change. The increasing number of available viral genomes that are provided by modern sequencing techniques allows us to conduct a genome-wide analysis for recent selective sweeps to gain insight into the within-host evolution and adaptation of human influenza A viruses.

Several methods were developed to detect and measure the effect of directional evolution for viral populations. We previously described Allele Dynamics (AD) plots, which characterize the evolutionary dynamics of sets of amino acid changes, indicating those most likely to be under positive selection using population level time-series data sets of genetic sequences[13]. Similarly, nextflu.org provides a web-based visualization of changes in allele or clade frequencies in the HA protein of circulating seasonal influenza viruses[14]. Related work from *Luksza and Lassig*[15] builds upon clade frequencies to forecast influenza lineages with acquired fitness advantages in the viral population. Other methods to analyze natural selection are based on non-synonymous to synonymous mutation rates (dN/dS)[16]. Synonymous changes are assumed to be neutral, while a relative excess of non-synonymous changes, i.e. $dN/dS > 1$, indicates positive selection[16]. dN/dS is either calculated by counting synonymous and non-synonymous substitutions[17,18] or by estimation using maximum likelihood models[17,19]. This statistic is not applicable to detect selective sweeps, as a large number of synonymous substitutions could occur after a substitution rose to fixation in a selective sweep, which would result into a dN/dS ratio smaller than 1 and the conclusion that this site is not evolving under positive selection[12]. Moreover, dN/dS was originally developed for the analysis of divergent species and the interpretation of $dN/dS > 1$ as positive selection may not be correct for single populations[20]. To elude the limitations of dN/dS, *Bhatt et al.* developed a statistic based on site frequencies to calculate site- or segment-specific adaptation rates[21]. Furthermore, several other approaches have been developed to identify selective sweeps using accelerated substitution rates[12], a skew in the allele frequency spectrum[19] or an excess of linkage disequilibrium[22]. Detecting the season or the time period in which a specific amino acid change involved in a selective sweep emerged, would improve comparative molecular studies of natural selection and indicate changes with potential effect on the viral fitness. This could aid to uncover the drivers of adaptive evolution in viral populations.

Here, we describe Sweep Dynamics (SD) plots, which allow analyzing the population-level phylodynamics of influenza virus proteins or proteins of other rapidly evolving organisms from longitudinal samples of genetic sequences. A statistical evaluation reveals selective sweeps, and in addition the season in which they occurred and the associated individual amino acid changes. We used the SD plots for a genome-wide characterization of directional selection in pH1N1 influenza viruses since their introduction into the human host. In all proteins under consideration, we inferred sweep-related changes that indicate human-adaptive changes after its emergence in 2009, several of which were in structural proximity to known mammalian host adaptation sites. Furthermore we detected sweep-related changes in antigenicity- and avidity-changing sites of the sH3N2 influenza virus hemagglutinin that correlate with newly emerging antigenic variants in the human population and show the value of SD plots for vaccine strain selection problem[9].

Results

Sweep Dynamic (SD) Plots.

Sweep Dynamics (SD) plots are an extension of the AD plot technique that we previously described[13]. SD plots analyze the evolutionary dynamics of alleles, representing individual amino acid changes within the viral population. The dynamics of reconstructed amino acid changes (alleles) in an homogeneous, constant-sized viral population can be described by a Fisher model[23,24]. This model is also considered valid with changing population sizes[25–27] and seasonal influenza virus populations have been modeled as homogenous due to their rapid spread around the globe[20]. Genetic drift and selection are acting on alleles, resulting in changes of allele frequencies (ratio of copies of one genetic variant relative to the population size)[28,29]. In this population, an allele under directional selection rises faster in frequency than alleles without a selective advantage. Amino acid changes (alleles) that increase in frequency swiftly over time are thus more likely to be under directional selection than other alleles with lower frequencies. We apply this criterion in the SD plots method together with a statistical evaluation, to pinpoint those amino acid changes that increase significantly faster in frequency than others and thus might provide a selective advantage. Changes are inferred under consideration of the evolutionary relationships, to consider their relatedness and avoid counting over changes resulting from denser sampling of specific parts of the viral population.

From the sequences for a particular protein from a viral population sample, a phylogenetic tree is inferred and amino acid changes in its evolution are reconstructed that map to the individual branches in the tree (Material & Methods). The frequencies of circulating isolates that have inherited a particular amino acid change are deduced from the phylogenetic tree by counting the number of viral isolates descending from the branch where a particular amino acid change was introduced. This is done separately for each season (Fig. 1A and B). Other than the AD-plots, which combine amino acid changes at different positions of the coding sequence into alleles when they share a branch or occur in close proximity in the phylogeny, SD plots analyze individual amino acid changes for their potential effect on viral fitness. The visualization of SD plots highlights these identified sweep-related changes and their variation in frequency over time. Specifically, the following procedure is carried out.

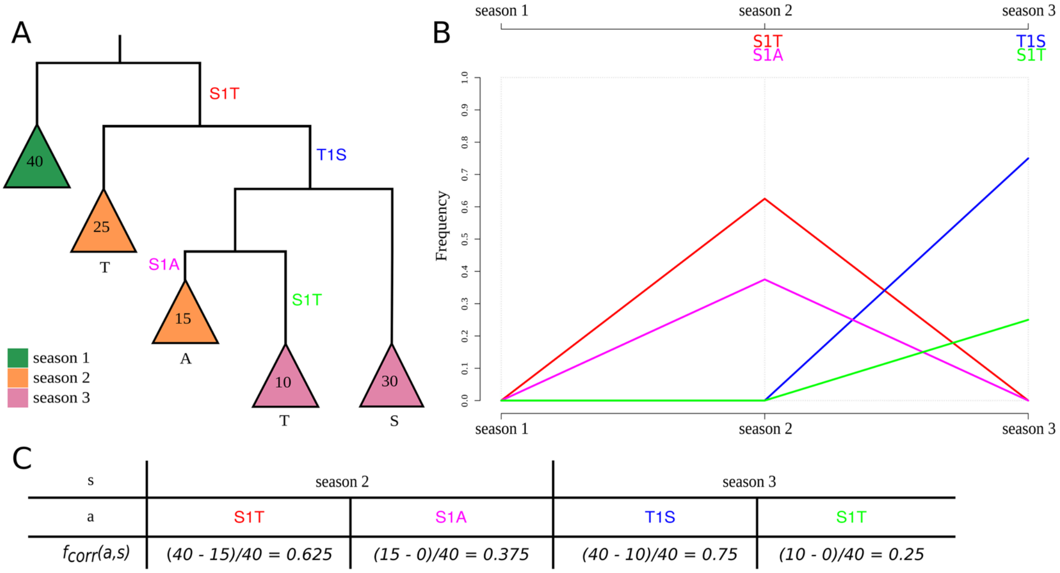

s	season 2		season 3	
a	S1T	S1A	T1S	S1T
$f_{corr}(a,s)$	(40 - 15)/40 = 0.625	(15 - 0)/40 = 0.375	(40 - 10)/40 = 0.75	(10 - 0)/40 = 0.25

Figure 1. Phylogeny demonstrating the frequency correction, the corresponding SD plot and frequencies of amino acid changes. This is a detailed illustration of how the frequency correction handles individual amino acid changes that occur at the same position. The tree T **(A)** consists of five main subtrees sampled from three seasons (colored in green, orange and purple). Each season s exhibits forty isolates ($|L_{T,\,s}| = 40\ \forall s$). A_T contains four amino acid changes that occur on different internal branches: S1T (red), T1S (blue), S1A (pink) and S1T (light green). We consider S1T (red) and S1T (light green) as two separate amino acid changes with individual frequencies as they occur on different branches of the tree. Consequently, both are calculated separately and occur in the SD plot **(B)**. Amino acid changes S1T (red) and S1A (pink) rise in frequency in the second season and disappear in the last season while T1S (blue) and S1T (light green) arise in the third season in the corresponding SD plot. Note that the frequencies for change S1T (red) and for T1S (blue) are corrected while the frequencies for S1A (pink) and S1T (light green) do not require a correction **(C)**.

Using a phylogenetic tree T and a set of reconstructed amino acid changes A_T for all internal branches, the frequency of isolates in the population that carry a specific amino acid change $a \in A_T$ is calculated as follows: let L_T represent the set of viral isolates assigned to the leaves in T, with each viral isolate $l \in L_T$ being labeled with a time stamp s indicating the season in which it was sampled and LT, s representing the subset of sequences of L_T labeled with time stamp s. Starting from the root, we perform a level order traversal, visiting each edge e in the tree T, and calculate the frequency for each individual amino acid change $a \in A_T$ that is located on the edge e as follows: Let T_a be the subtree that is rooted at the node with the in-edge e. Let A_{Ta} be the set of amino acid changes in the subtree T_a, with $A_{Ta} \subset A_T$ and $a \in A_T \wedge a \notin A_{T_a}$. The frequency $f(a, s)$ of an individual amino acid change a in season s is defined as: $f(a,\ s) = \frac{|L_{T_a,s}|}{|L_{T,s}|}$. It represents the ratio of all isolates in the subtree that have acquired the amino acid change a within season s relative to the number of all isolates within the designated season s.

As we consider individual positions, the prevalence of one amino acid change per position is affected by the emergence of a more recent amino acid change at the same position, making it necessary to adjust the frequency $f(a, s)$ at position p in the alignment. The frequency $f(a, s)$ of a occurring at position p is adjusted when another amino acid change β occurs at p in the subtree T_a — a process referred to as frequency correction, as follows: let there be n amino acid changes at p in the subtree T_a, i.e. $|A_{T_a}| = n$. Each subtree τ_β is rooted at the node with the in-edge that represents the amino acid change $\beta \in A_{T_a}$. The set $\left\{\tau_\beta \mid \beta\ \in A_{T_a}\right\} = X_{T_a}$ represents the n subtrees that are contained in the tree T_a. Let $L_{X_{T_a},s} = \cup_{\tau \in X_{T_a}} L_{\tau,s}$ be the set of all leaves with the time stamp s in all subtrees in X_{T_a}. Note that $L_{X_{T_a},s} \subseteq L_{T_a,s}$. The corrected frequency $f_{corr}(a,\ s)$ of amino acid change a in season s is then defined as: $f_{corr}(a,\ s) = \frac{|L_{corr}(T_a,\,s)|}{|L_{T,s}|}$, with $L_{corr}(T_a,\ s) = L_{T_a,s} - L_{X_{T_a},s}$. The frequency of an amino acid change a is adjusted by excluding isolates $L_{X_{T_a},s}$ that are subject to a more recent substitution (Fig. 1). The SD plots always apply $f_{corr}(a, s)$ because either the frequency needs to be corrected or whenever no additional amino acid change occurs in the phylogenetic tree T after the amino acid change α, the term $|L_{X_{T_a},s}|$ is zero and automatically results in the uncorrected case ($f(a, s)$). Thus, the equation $f_{corr}(a,\ \ s)\ \le\ f(a,\ \ s)$ holds. Note that this allows an individual analysis of the same amino acid exchange introduced several times in the phylogeny on different branches (e.g. S1T (red & light green) in Fig. 1) and their distinct evolutionary trajectories.

To identify a selective sweep and the associated amino acid change, we define two criteria: an amino acid change should show a significant increase in frequency relative to the previous season. For each season, we only report changes that were not reported as significant before. For each amino acid change, we test the null hypothesis that the number of viruses in the viral population carrying this change is equal or lower than in the previous season. We evaluate the significance of frequency changes for each amino acid change a using Fisher's exact test[30], using $|L_{corr}(T_a, s)|$ and $|L_{corr}(T_a, s+1)|$ over consecutive seasons s and $s+1$. A significant p-value ($p \leq 0.05$) indicates that an amino acid change significantly increased in frequency in the current season relative to the previous one. To correct for multiple testing, we adjusted the p-values with the Benjamini-Hochberg procedure controlling the false discovery rate at level $\alpha = 0.05$[31].

For each dataset, the seasons from the second to the last one are tested, comparing each season to the preceding one. We report amino acid changes for the season s of their first predominant occurrence ($f_{corr}(a, s) > 0.5$; it occurs in more than 50% of the isolates within the designated time period) as in Steinbrück and McHardy[13] in combination with a significant p-value ($p \leq 0.05$).

The results are visualized in SD plots (Figs 2 and 3). These provide a detailed overview of the emergence of individual amino acid changes in the viral population and in which season a sweep took place. The changes in frequency of sweep-related changes are depicted as trajectories over consecutive seasons. The season of their first predominant occurrence is indicated with an asterisk. In each season, the amino acid exchanges of all sweep-related alterations are listed in a panel above the graph. Within the panel, they are bottom-up ordered with ascending frequency.

Selective sweeps in the evolution of pH1N1 influenza viruses. We applied SD plots to detect selective sweeps in the past evolution of pH1N1 influenza viruses. We analyzed nucleotide and amino acid sequences of ten proteins (HA, NA, M1, M2, NS1, NS2, NP, PA, PB1 and PB2) collected since the appearance of the virus in the beginning of 2009 until the end of September 2015[2]. Sequences were assigned to influenza seasons using the common definitions for seasons in the Northern and Southern hemisphere (Data & Methods). For pH1N1 influenza, the data covered fourteen seasons from 2009N to 2015S (Fig. 2, Supplementary Table 1). To investigate the structural relationships of sweep-related changes in the proteins, we mapped sweep-related changes in HA1, NA, NP and the polymerase (PB1, PB2 and PA) onto the respective structures (Material and Methods).

The SD plots analysis indicated selective sweeps and associated changes for the 2009S, 2011N, 2012N, 2013N, 2013S, 2014N, 2014S and 2015N seasons. The most sweep-related changes (twelve and seventeen, respectively) were detected for the surface proteins HA and NA and the fewest were found for NS2 (two changes) over all thirteen seasons. Newly arising changes often occurred simultaneously, i.e. were detected in the same season, with up to five changes detected in a protein in one season (2013S in PA and NA, 2013N in PB2), and with changes occurring simultaneously in multiple proteins (Fig. 2). In addition to changes providing a selective advantage, some of these are likely hitchhikers without notable effect on fitness. With hitchhikers, we refer to (almost) neutral changes that are introduced into a sequence shortly before or after a change causing a selective sweep. Hitchhikers then rise in frequency together with beneficial changes due to genomic linkage and are thus detected as being sweep-related. Technically, the simultaneous occurrence of amino acid changes on the same branch prevents a computational distinction between their potential effects, as they are ancestral to the same set of leaf nodes. Besides linkage within a genomic segment, there is also a strong linkage across all influenza segments[32–34], resulting in hitchhikers from other segments being carried along to higher frequencies by functionally relevant changes. The visualization of evolutionary dynamics in the SD plots can identify some of these 'sweep-related hitchhikers' as those decreasing in frequency after their appearance in a sweep, due to a reassortment event or another substitution, and not becoming fixed.

For the 2009S season, we detected a selective sweep at seven amino acid positions throughout the viral genome (in PA (L581M), HA (S203T) (position 202 in *Otte et al.*[35]), NP (V100I, I373T), NA (V106I, N248D) and NS1 (I123V)) (Fig. 2C,D,E,F and I, Supplementary Table 1), which were also described in *Otte et al.*[35]. All of these changes rapidly became predominant in this season and continued to rise in frequency until they were close to fixation in 2010N, suggesting that the new amino acid was present in nearly all sampled isolates in this season. These findings are in agreement with the study of *Elderfield et al.*, in which 2009S was identified as the time of the first wave of pH1N1 activity after its emergence[36]. The pandemic waves were defined based on large viral prevalence with a phase of low viral prevalence in between. Five of seven detected sweep-related changes were also described in this study as emerging changes in the first wave of the pandemic, with frequencies close to 100% in the second wave in 2010N, similar to the frequencies we observed in our analysis (frequencies between 91% and 99%, with slight differences most likely due to differing time frames and datasets in both analyses). With the exception of the V106I and N248D changes in NA, all sweep-related changes detected in 2009S were still fixed in the population in 2015. The frequency of the amino acid change V106I in NA decreased from 2011S onwards, as it was replaced by the I106V sweep-related change in 2013N. The frequency of V106I accordingly dropped rapidly from 78% to 11% between 2012S and 2013N and continued to decrease until it disappeared in 2014S. From 2011S onwards, the frequency of N248D also decreased to 0% in 2014S. This amino acid change re-emerged in 2013N and replaced the strain with the first change. This repeated emergence indicates a particular relevance of this change regarding viral fitness. All seven sweep-related changes detected in 2009S have been reported to induce functional changes that might have facilitated viral adaptation to the human population: we previously described that all changes with the exception of NS I123V mediated increased pH1N1 influenza virus pathogenicity in a mouse model[37]. Moreover, all seven adaptive mutations were associated with enhanced respiratory droplet transmission in a ferret model, suggesting their crucial role to sustain with the mammalian host[35]. The ability of influenza A viruses to transmit from human-to-human is considered to be key in pandemic spread. Hereby, particularly the receptor binding properties of HA play an important role. We have also previously shown that HA S203T increases binding to α2,6-linked sialic acids (corresponds to position 202 in *Otte et al.*[35]) that are predominantly expressed in the upper respiratory tract of humans, a key site in virus transmission among humans[35,38,39].

Both residues I100 and T373 in NP are solvent exposed ($RAS = 0.32$ and $= 0.26$, respectively); T373 is in close proximity to N319 (10.2 Å measured from Cα to Cα, Fig. 4A), at which an N to K change promotes adaptation to mammalian cells[40]. Elevated virulence was also found for substitutions V106I in NA and I123V in NS1[41]. The

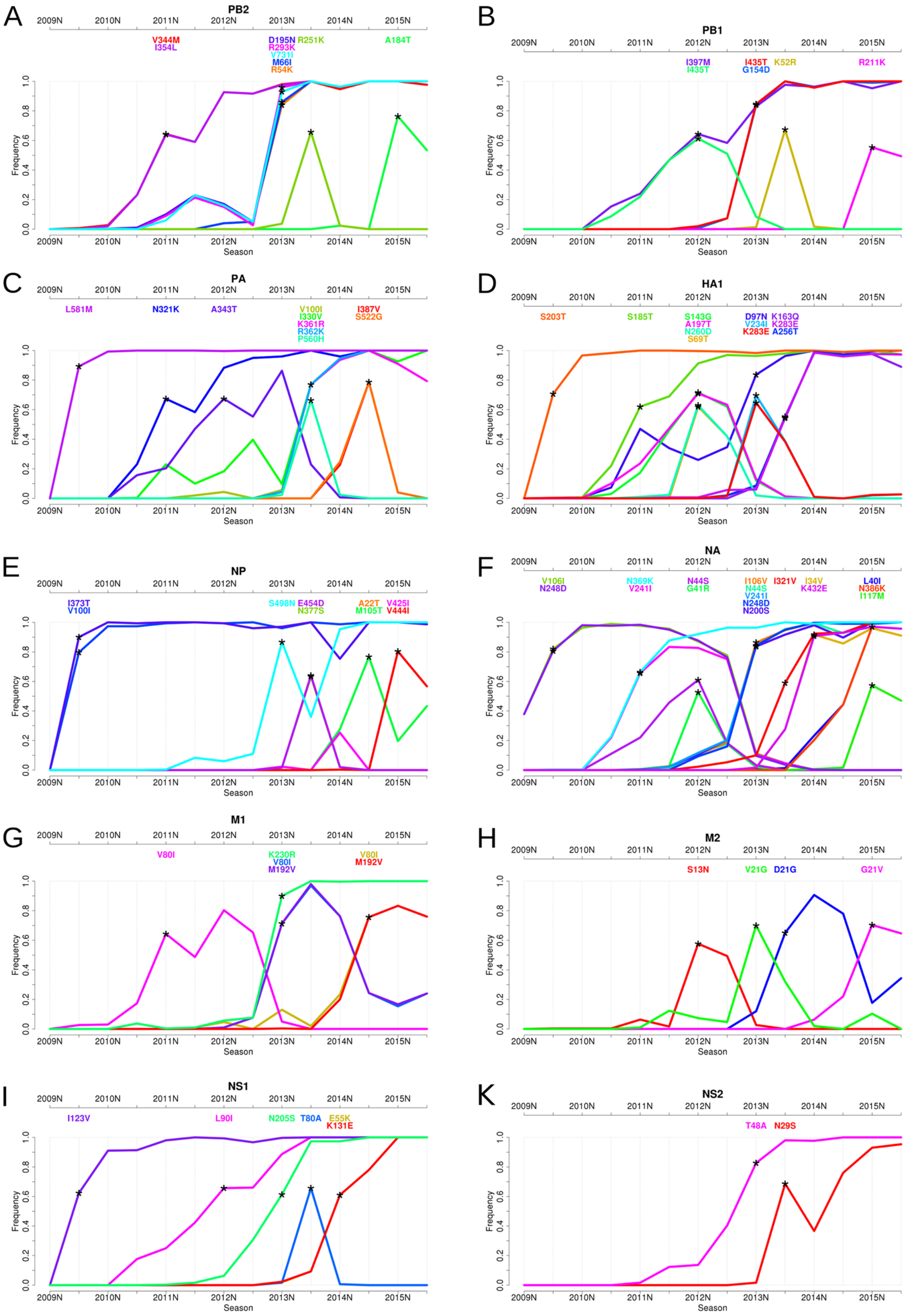

Figure 2. Sweep Dynamics (SD) plots for ten pandemic H1N1 influenza A proteins. These plots show the alterations in frequency of sweep-related changes over consecutive time periods in the proteins PB2, PB1, PA, HA, NP, NA, M1, M2, NS1 and NS2. They are ordered from **(A)**–**(K)** based on decreasing segment size on which they are encoded. Each plot shows the seasons (from 2009S to 2015S) on the x-axis and the frequency on the y-axis. The initial emergence of a sweep-related amino acid change is indicated by an asterisk pinpointing the first season in which it significantly rises in frequency to a frequency of more than 50%. Sweep-related changes are listed in a panel above the graph and are identically color coded as the curve in the plot. Within the panel, they are bottom-up ordered with ascending frequency.

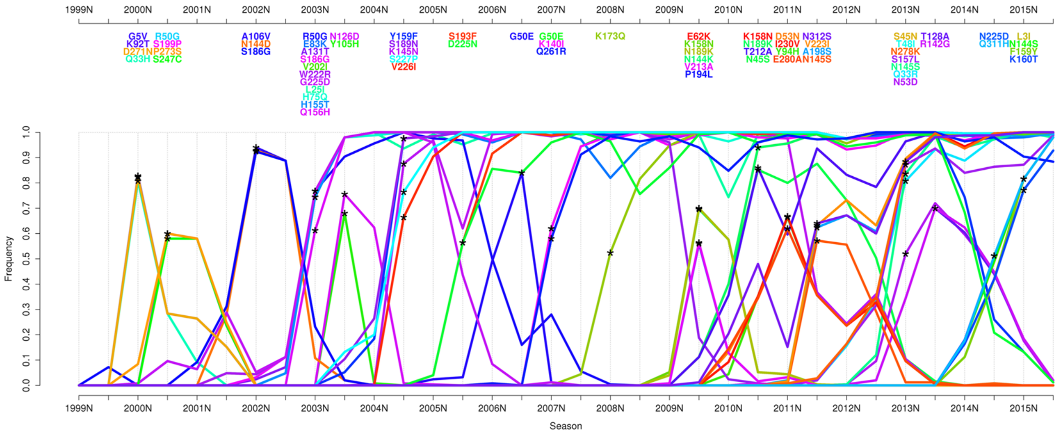

Figure 3. Sweep Dynamics (SD) plot for the seasonal H3N2 influenza A hemagglutinin. This plot shows alterations in frequency of sweep-related changes over consecutive time periods for the influenza A/H3N2 hemagglutinin. It depicts the seasons (from 1999S to 2015S) on the x-axis and the frequency on the y-axis. Sweep-related changes are listed in a panel above the graph and are identically color coded as the curve in the plot. Within the panel, they are bottom-up ordered with ascending frequency.

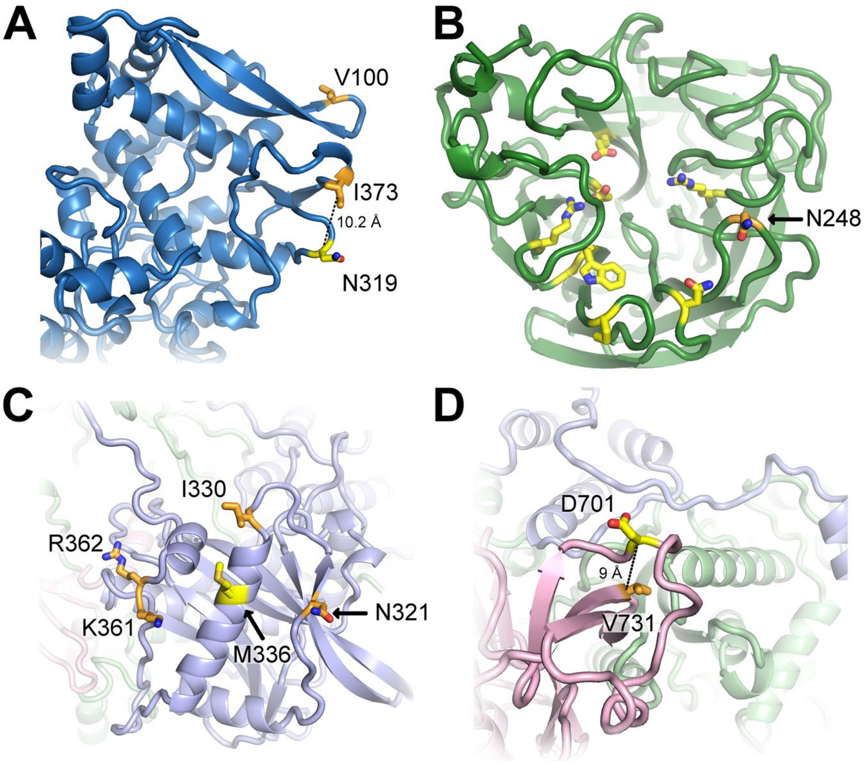

Figure 4. Representation of sweep-related changes on protein structures. We mapped individual sweep-related changes on the corresponding models shown as cartoon with interesting residues shown as sticks and colored by atom-type (yellow and orange for carbon, red for oxygen and blue for nitrogen). In **(A)**, the structure of NP is shown in blue with sweep-related mutated residues T373 and I100 colored orange and mammalian-adaptation site N319 yellow. The distance between Cα-atoms of T373 and N319 is 10.2 Å (dotted line). The structure in **(B)** depicts NA (green) with residue N248 (orange) in proximity (<12 Å) to the active center (yellow)[42]. In **(C)** and **(D)** we show views on the structural model of the polymerase with subunits PB2 (pink), PB1 (light green) and PA (light blue). Sweep-related changes at residues N321, I330, K361 and R362 (orange) in PA cluster around M336 (yellow) that increases polymerase activity in mammalian cells **(C)**[46]. The structure of polymerase subunit PB2 (pink) is shown in **(D)** and highlights the sweep-related mutation V731 (orange), which is in close vicinity (≤9 Å) to position 701 that enhances mammalian host adaptation[40,49].

V106I and N248D substitutions enhance viral stability at low pH, which confers replicative fitness and likely promotes virus spread[42]. Notably, through the N248D change, the protein acquires a negative charge (at neutral pH) that is solvent-exposed ($RSA = 0.56$) and located within <12Å vicinity to residues belonging to the three-dimensional structure of the active center of NA[43,44] (Fig. 4B).

We detected a second selective sweep in season 2011N, corresponding to the third wave of the pandemic[36]. We identified seven accompanying changes in PB2, PA, HA, NA and M1 (Fig. 2A,C,D,F and G, Supplementary Table 1). The changes V244M and I354L (PB2), N321K (PA), S185T (HA) and N369K (NA) came close to fixation in later seasons, with frequencies of around 90% in 2012N. Notably, their rise in frequency was slower in comparison to the changes from 2009S, which reached a frequency of nearly 100% only one season after they were detected. The change S185T in HA was reported to enhance receptor binding avidity[45], while N321K in PA increased polymerase activity[36]. This residue is exposed on the structure ($RSA = 0.41$) and close to M336 (Fig. 4C), which was reported to foster adaptation by increasing polymerase activity in mammalian cells[46]. Furthermore, the amino acid changes N369K and V241I in NA were described as permissive mutations which enhanced viral fitness in oseltamivir resistant viruses[47]. As the amino acid change V241I decreased in frequency in 2013N (Fig. 2F) and is buried in the protein ($RSA = 0$), this could indicate that site N396K (exposed, $RSA = 0.1$; uncharged to positively charged) might be the key amino acid change that confers antiviral resistance.

After the third global wave in 2011N, the pH1N1 influenza virus continued to circulate in the human population with lower activity throughout 2012 in a wide range of countries, especially in Europe and Eastern Asia[48]. The SD plots indicated a selective sweep in 2012N accompanied by eleven changes in the proteins PB1, PA, HA, NA, M2 and NS1 (Fig. 2B,C,D,F,H and I, Supplementary Table 1). Eight of these changes (I435T in PB1 and all changes in HA, NA and M2) decreased in frequency right after this selective sweep and disappeared completely in 2013S. The A343T change in PA also was lost a year later in 2014S. This behavior is striking in comparison to the previously detected sweeps in 2009S and 2011N, where a majority of sweep-related changes became fixed (except V241I (NA) and V80I (M1)). For the selective sweep in 2012N, only the I397M amino acid change in PB1 and the L90I amino acid change in NS1 continued to be present in the circulating viral population and became fixed in 2013S (Fig. 2B and I), suggesting their relevance for the sweep while the remaining changes could have been hitchhikers subsequently lost by reassortment events.

In 2013N, the pH1N1 influenza virus re-emerged with more activity in the countries where activity was low in 2012[48]. Here the SD plots revealed twenty-two sweep-related changes in all proteins, except for PA (Fig. 2, Supplementary Table 1). PB2 and NA had the most changes, with five amino acid changes each rising rapidly in frequency and coming close to fixation within one season. Seventeen of these twenty-two amino acid changes were still fixed at the end of 2015S, suggesting that some of these changes provide a selective advantage. The sweep-related change V731I (PB2) is located in the vicinity (9Å) of residue 701 (Fig. 4D), a position known to be involved in mammalian host adaptation[40,49]. Further sweep-related changes not rising to fixation occurred in HA (V234I and K283E), M1 (V80I and M192V) and M2 (V21G).

We detected a sweep in 2013S with sixteen sweep-related changes in nine proteins, with six changes in PB2 (R251K), PB1 (K52R), PA (P560H), NP (E454D and N377S) and NS1 (T80A) decreasing quickly in frequency and showing frequencies close to 0% one season after their emergence. The other sweep-related changes were still fixed in the viral population in 2015S and thus could be of functional relevance, including V100I, I330V, K361R and R362K in PA, K163Q, K283E and A256T in HA and I321V in NA (Fig. 2C,D and F). Especially the changes I330V, K361R and R362K in line with N321K (season 2011N) cluster significantly around the mammalian-adaptation site 336 on the structure of PA that increases polymerase activity (Fig. 4C)[50]. This might suggest that these PA changes might also affect viral polymerase activity, as a hallmark of influenza disease severity in humans. We tested for enrichment of fixed sweep-related sites within a radius of <13Å in the vicinity of site 336 (hypergeometric distribution; $N = 716$, $K = 31$, $n = 6$, $k = 4$; H_0: fixed sweep-related changes occur with the same probability in vicinity to site 336 and in the remaining protein region; $P = 4 \times 10^{-5}$; N being all sites in the protein model, K the median number of sites in a radius of 13Å around a site in the protein model, n all detected sweep-related changes which remained fixed, k the number of fixed sweep related changes in the cluster). The change K283E in HA (site 283 is exposed; $RSA = 0.41$) results in a change of charge from positive to negative and is located in the stalk region that plays a key role in the induction of neutralizing antibodies[51].

The 2014N and 2014S seasons showed sweep-related changes only for a small number of proteins. In 2014N, two changes were detected in both NA and NS1 (Fig. 2F,I), which all rose to fixation and still circulated in 2015S. In 2014S, changes in the proteins PA, NP and M1 were identified subsequently. While I387V and S522G in PA disappeared in 2015S, M105T and A22T in NP were maintained at frequencies of around 40% (Supplementary Table 1). The V80I and M192V changes in M1 were already detected in 2013N, but disappeared due to back mutations and re-emerged, indicative of a functional relevance.

Similar to 2013S, many sweep-related changes detected in 2015N decreased in frequency in 2015S. Exceptions are L40I and N386K in NA, which remained close to fixation in 2015N and seem most likely to provide a selective advantage. Six sweep-related changes in PB2 (A184T), PB1 (R211K), NA (I117M), NP (V425I, V444I), M2 (G21V) decreased in frequency but still remained predominant, with frequencies around 50% or higher in 2015S (Fig. 2A,B,D,E and H, Supplementary Table 1).

In addition, we investigated the effect of data sampling for the HA protein (Data & Methods). The SD plots analysis was repeated on all data deposited in the EpiFlu database, which yielded similar results with a majority of sweep-related changes occurring in both datasets (Supplementary Table 3). A notable difference was the S203T substitution, which was not detected in the unsampled dataset, but is known to be relevant for the adaptation of pH1N1 at the beginning of the pandemic in 2009[35,37]. Since only 2 isolates are available for 2009N, S203T is not significant in the unsampled data, although the frequencies are similar. A more fine-grained resolution, i.e. by calculating frequencies per month and not per season, should still identify S203T as a sweep-related change[13].

Selective sweeps in the evolution of sH3N2 influenza. To investigate the past evolution of the seasonal sH3N2 influenza virus, we analyzed sequence data of the 34 seasons from 1999N to 2015S. The sH3N2 influenza virus has been circulating in the human population since 1968, but before 1999N sequence data only few data are available. In the SD plots analysis we therefore focused on more recent years, ensuring a sufficient data coverage for each season (Fig. 3, Supplementary Table 2).

Overall, we identified fifteen seasons in the analyzed time period with sweep-related changes in the HA protein. For each detected selective sweep, we investigated whether it indicated the emergence of an antigenically novel strain that became predominant by matching the sweep-related changes to the amino acid changes that were reported for the viral strain by the WHO. If not stated directly for the predominant strain, the changes reported for the subclade including the predominant strain were used for matching to the WHO reported strains, as they distinguish a novel viral variant from previous ones. We further assessed the coherence between detected selective sweeps and novel antigenic variants by comparing the sweep-related sites to known antigenicity- and avidity-changing sites. We recently reported twenty-three antigenicity-altering sites organized in five patches on the structure of HA playing a role in the past antigenic evolution of sH3N2 viruses[52], a subset of which together with position 193 were also reported by *Koel et al.*[53]. Of the sites influencing the receptor binding properties, i.e. avidity changing, we focused on the sites 193, 222 and 225[54], as well as 145[55], which is also an antigenicity-altering site[52], bringing the set of considered sites to twenty-six.

Of the fifteen seasons in which sweep-related changes were detected in the HA protein, eleven included changes at these twenty-six sites (Fig. 5). Of the eleven sweeps with relevant changes, three matched and indicated the emergence of a novel antigenic variant one season before the strain became predominant (A/Fujian/411/2002 strain, A/California/7/2004 strain and A/Perth/16/2009 strain) (Fig. 5). In two cases, a newly emerging strain was matched and detected two seasons before predominance (A/Wisconsin/67/2005 and A/Brisbane/10/2007) (Fig. 5). This is ideal for vaccine strain selection, as new strains to be included in the vaccine formulation are decided on one year in advance. Three cases matched and indicated a newly emerging strain in the season in which it was predominant (A/Victoria/208/2009, A/Texas/50/2012 and A/Hong Kong/4801/2014). Interestingly, for two strains (A/Brisbane/10/2007 and A/Hong Kong/4801/2014) we identified the associated sweep-related changes over two consecutive seasons. Only the appearance of the A/Victoria/361/2011 strain coincided with a sweep without changes at known antigenicity or avidity sites (Fig. 5), which indicates that our list of antigenicity or avidity altering sites likely is not complete. The four sweeps without changes in antigenically- and avidity-altering sites did not include changes observed for antigenically novel predominant strains reported by the WHO.

In comparison to the strain recommendations by the WHO, sweeps predicted with the SD plots and including changes at antigenicity- or avidity altering sites identified newly emerging strains at the same time in three cases (e.g. A/Fujian/411/2002) or up to two seasons before in six cases (e.g. A/Brisbane/10/2007; Fig. 5). Notably, the SD plots analysis did not identify sweeps corresponding to A/Wellington/1/2004 and A/Switzerland/9715293/2013, which were false positive vaccine strain recommendations that did not match the dominantly circulating strain[56–58]. In some cases practical issues such as the lack of a vaccine strain with sufficient growth properties in eggs, which might have prevented recommendation of a suitable vaccine strain candidate by the WHO. SD plot analysis indicated suitable strains in the majority of cases using a fixed computational procedure, and therefore seems suitable for supporting the vaccine strain decisions of the WHO experts. Notably, different from the established WHO procedure, no interpretation of hemagglutination inhibition assay data was required for this result. This could be an additional benefit, as recently, HI assays fail to agglutinate many circulating sH3N2 viruses[59].

To evaluate the effect of sampling the data to generate the same number of sequences per season (Data & Methods), we repeated the SD plots analysis for the HA protein on full datasets. For sH3N2, sixty of the sixty-nine sweep-related changes detected in the previous analysis (Fig. 3) were also identified in the unsampled data (Supplementary Table 4). Of the changes not detected in the unsampled data, only the G50E change in 2006S and 2007N is relevant for the vaccine update to recommend the A/Brisbane/20/2007 strain (Fig. 5). G50E actually shows similar frequencies in both sampled and unsampled data, but the statistical test lacks power to detect this change due to a very low number of sequences in 2006S. With the more extensive data coverage in recent years, this should not be an issue for the application of our method in future seasons. Only three substitutions are found additionally in the unsampled data, which leads to the conclusion that the sampling is sufficient to represent circulating sH3N2 viruses.

We further applied the SD plots to sequences collected prior to the WHO meeting of the respective seasons. In this scenario, we produced a genealogy and accompanying SD plot for each season, thus excluding data from later time points also from tree inference. Except for minor differences in sweep-site detection and occasionally altered frequencies, this did not alter the suggested updates of the vaccine strains obtained when analyzing a tree generated across the entire time period (Fig. 5). The plots are provided at https://github.com/hzi-bifo/SDplots[60].

Discussion

We describe a new method and software called SD plots that combines phylogenetics with a statistical analysis to detect selective sweeps and associated individual amino acid changes under directional selection from longitudinal samples of population-level sequence data. Due to the rapid evolution of influenza viruses, backmutations or repeated mutations at individual sites are common in certain protein regions, requiring elucidation of the evolutionary histories of the proteins to distinguish between different evolutionary events. An important aspect of the SD plot method is that it suggests individual amino acid changes that might be under directional selection, instead of sites. It thus gives a more fine-grained view on the potential influence of individual changes; for instance for the same change occurring in distinct genetic backgrounds, or of different changes occurring at the same position.

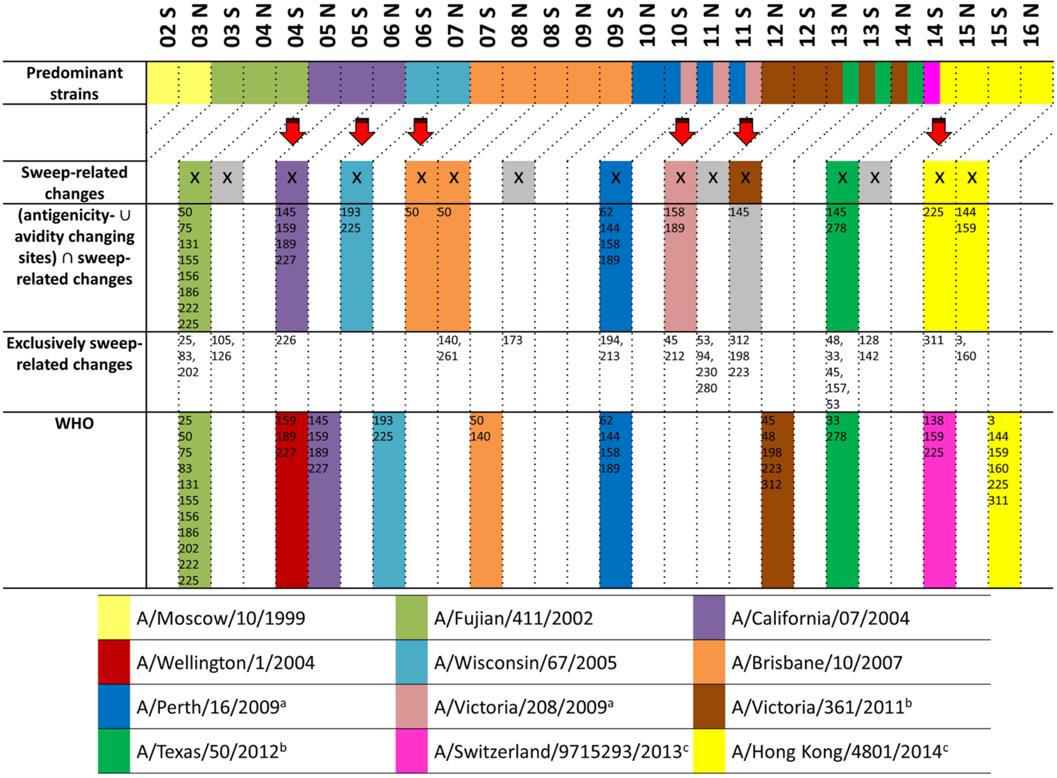

Figure 5. Comparison of predominant seasonal H3N2 influenza A strains, SD plots results and recommendations made by the WHO. From 1999N until 2015S, eleven antigenically different sH3N2 influenza strains were selected for production of the seasonal influenza vaccine, named Moscow/10/1999, A/Fujian/411/2002, A/Wellington/1/2004, A/California/7/2004, A/Wisconsin/67/2005, A/Brisbane/10/2007, A/Perth/16/2009, A/Victoria/361/2011, A/Texas/50/2012, A/Switzerland/9715293/2013 and A/Hong Kong/4801/2014[2,79–87], which are indicated by colors as labeled in the legend (first row). For the SD plots analysis, seasons are marked (with an X in the second row) if sweep-related changes distinguish the respective vaccine strain from the previous one. False positive or false negative results are marked in grey. The third row lists sweep-related changes that also are antigenicity or avidity changing sites, while the fourth row shows detected sweep-related sites that are neither known to change the avidity or the antigenicity. The selection of a vaccine strain takes place two seasons before the vaccine is available. Any prediction of newly arising antigenically novel strains should therefore not be compared to the current predominant strain, but to the predominant strain two seasons after the detection. This comparison of the WHO selections and the SD plots results with the predominant strain two seasons later is indicated by the diagonal lines in the upper part of the plot (fifth row). [a]The strain A/Victoria/208/2009 was predominant in 10 S, 11 N and 11 S but was antigenically indistinguishable from A/Perth/16/2009[3,88,89]. [b]The strains A/Victoria/361/2011 and A/Texas/50/2012 were predominant in 13 N, 13 S and 14 N but A/Texas/50/2012 was antigenically more effective[85,90,91]. [c]In 14S, two different clades containing the strains A/Switzerland/9715293/2013 and A/Hong Kong/4801/2014, respectively, were rising in frequency at the same time and antigenically differed from the previous vaccine strain A/Texas/50/2012[86].

For pH1N1 viruses, the SD plots identified sweep-related changes that clustered on the protein structure together with known host adaptation sites, indicating their potential relevance for this process, which makes them interesting for experimental studies. For the polymerase proteins these "adaptation patches" include changes known to increase polymerase activity in mammalian cells and to promote adaptation to the human host since the establishment of pH1N1 in 2009. Specifically, wet-lab experiments could focus on position 731 in the pH1N1 PB2 protein (a potential novel adaptation site), positions 330, 361 and 362 in pH1N1 PA and positions 54, 66 in pH1N1 PB2 (potentially promoting polymerase activity). For sH3N2 viruses, most sweep-related changes identified in HA occurred at known immune evasion sites.

The identification of selective sweeps in the SD plots with changes in antigenic patch sites or avidity changing sites allowed the timely detection of newly emerging antigenic variants for the sH3N2 viruses. Using these as suggested updates of the vaccine strain resulted in a better match to future predominant strains than the strains recommended by the WHO, also in a retrospective testing scenario, when we used only isolates with a sampling date prior to the respective vaccine selection meeting. The latter is the most realistic set up for testing the value of vaccine strain predictions, as it considers primarily the available data from the EpiFlu database (http://platform.gisaid.org) for the vaccine selection meeting of the WHO. A complete overview of isolated and submitted sequences per season is available at https://github.com/hzi-bifo/SDplots[60]. To evaluate the performance of the SD plots for the vaccine strain prediction under similar conditions to the WHO, we are planning to analyze the data deposited in the EpiFlu database before the vaccine strain selection meeting every season and publish the results at https://github.com/hzi-bifo/SDplots_VaccineUpdates[61]. Given that there are no substantial population bottlenecks, which would accelerate fixation of changes due to genetic drift, SD plots could also be used to study the predict selective sweeps and implicated amino acid changes for of other rapidly evolving pathogen populations from longitudinal sequence samples.

Data and Methods

Data download and sampling.

Protein and nucleotide coding sequences were downloaded from the NCBI flu database[62]. For both the pH1N1 influenza and sH3N2 influenza subtype, we downloaded sequences of the proteins HA, NA, M1, M2, NS1, NS2, NP, PA, PB1 and PB2. HA sequences were additionally downloaded from the GISAID database[63] to evaluate the effect of sampling the data. The pH1N1 influenza virus was analyzed from the emergence of the virus in early 2009 until the end of September 2015, while sH3N2 influenza was studied from October 1998 until the end of September 2015. We downloaded sequences with the full date available, to properly assign sequences to influenza seasons. We used the standardized definition for the Northern hemisphere season (N) that begins on 1st October of the previous year and ends on 31st March and the Southern hemisphere season (S) that begins on 1st April and ends on 30th September in the same year, as before[13].

We limited our analysis to isolates represented by both a nucleotide and a corresponding amino acid sequence. To account for variable numbers of sequences per season, we sampled the data with replacement, generating the same number of sequences per season for our analysis (300 sequences for pH1N1, 250 sequences for sH3N2). For HA, the amino acid numbering based on the mature protein without the signal peptides was used; corresponding to seventeen and sixteen amino acids for pH1N1 influenza viruses and sH3N2 influenza viruses, respectively[64,65]. In an additional experiment, we used only sH3N2 isolates with a collection date prior to the respective vaccine selection meeting for each season individually and calculated the genealogy and SD plots.

Alignment and Phylogenetic inference.

We generated multiple sequence alignments from both the nucleotide or amino acid sequences with MUSCLE[66]. To avoid shifts in the numbering of both alignments, positions with gaps in more than 80% of the sequences are removed from the alignment with TrimAl[67]. A phylogenetic tree was inferred from the nucleotide alignment using fasttree[68] with the GTR-model, which enables a quick tree computation for large numbers of sequences while retaining a good accuracy compared to slower methods. For the pH1N1 influenza virus subtype, the A/California/05/2009 strain and for the sH3N2 influenza virus subtype the A/Moscow/10/1999 strain were used as an outgroup to root the trees. Both viruses were predominantly circulating in the viral population in the first season of our analyses[2,69]. We resolved multifurcations by adding further nodes and zero length edges into the outgoing edges to obtain a binary representation of the tree and subsequently applied the parsimony model of Fitch's algorithm with accelerated transformation (ACCTRAN)[70] to reconstruct amino acid sequences for the internal nodes of the phylogenetic trees. Amino acid changes were then inferred from the node-associated amino acid sequences and mapped to branches of the tree.

Protein structure analyses.

To investigate the structural properties of sweep-related changes, we mapped all sweep-related changes in HA1, NA, NP and the polymerase (PB1, PB2 and PA) onto the respective structures. For NA, the crystal structure of the A/California/07/2009(H1N1) strain (PDB 4B7Q) was used that covers residues 83–469 of NA. For HA1 and NP, we generated homology models based on structures from the RSCB database and the amino acid sequence of the A/California/07/2009(H1N1) strain using MODELLER[71,72]. Multiple sequence alignments containing protein templates and target sequences for modeling were calculated with MUSCLE[66]. Two structures (PDB 3M6S and 3LZG) from the A/Darwin/2001/2009(H1N1) strain displaying a sequence identity of 99.07% within residues 1–322 compared to the A/California/07/2009(H1N1) sequence were used as templates for composite modeling. For NP, we used the crystal structure of NP from the A/Wilson-Smith/1933(H1N1) strain (PDB 3RO5) with an identity of 91.9% compared to the A/California/07/2009(H1N1) strain. To obtain a three dimensional model of the viral polymerase, we generated individual models of PA, PB1 and PB2 for the A/California/05/2009(H1N1) strain using the Phyre II server[73]. These models were subsequently superposed onto the structure of the intact influenza A polymerase of *Reich et al.*[74] (PDB 4WSB).

We determined the exposure of each site with the tool SURFACE from the CCP4 toolkit[75,76] and calculated the accessible surface area (ASA), using a 1.4 Å radius for the probe sphere equal to the radius of water and the van der Waals radii for different types of atoms defined by Chothia[77], as well as a step variable of 0.1. To calculate the relative solvent accessibility (RSA), we normalized ASA values with a theoretical value of the maximum possible solvent accessibility and classified residues as buried when the RSA is ≤ 0.05 and as exposed otherwise[78].

Data and Software Availability.

The SD plots software, the figure and tables from this manuscript, and all related data used in this publication are fully available under: https://github.com/hzi-bifo/SDplots.

References

1. WHO. *Fact sheet number 211*, (2014).
2. WHO. Recommended composition of influenza virus vaccines for use in the 2010 influenza season. *WHO Weeky Epidemiological Record* **84**, 421–436 (2009).
3. WHO. Recommended composition of influenza vaccines for use in the 2012 southern hemisphere influenza season. *WHO Weekly Epidemiological Record* **86**, 457–468 (2011).
4. Wise, H. M. *et al.* Identification of a novel splice variant form of the influenza A virus M2 ion channel with an antigenically distinct ectodomain. *PLoS pathogens* **8**, e1002998, https://doi.org/10.1371/journal.ppat.1002998 (2012).
5. McHardy, A. C. & Adams, B. The role of genomics in tracking the evolution of influenza Avirus. *PLoS Path.* **5**, e1000566–e1000566, https://doi.org/10.1371/journal.ppat.1000566 (2009).

6. Medina, Ra & García-Sastre, A. Influenza A viruses: new research developments. *Nature Reviews Microbiology* **9**, 590–603, https://doi.org/10.1038/nrmicro2613 (2011).
7. Smith, D. J. *et al*. Mapping the antigenic and genetic evolution of influenza virus. *Science* **305**, 371–376, https://doi.org/10.1126/science.1097211 (2004).
8. Russell, C. A. *et al*. Influenza vaccine strain selection and recent studies on the global migration of seasonal influenza viruses. *Vaccine* **26**(Suppl 4), D31–D34, https://doi.org/10.1016/j.vaccine.2008.07.078 (2008).
9. Klingen, T. R., Reimering, S., Guzman, C. A. & McHardy, A. C. In Silico Vaccine Strain Prediction for Human Influenza Viruses. *Trends in microbiology*, https://doi.org/10.1016/j.tim.2017.09.001 (2017).
10. Bouvier, N. M. & Palese, P. The biology of influenza viruses. *Vaccine* **26**(Suppl 4), D49–53 (2008).
11. Vitti, J. J., Grossman, S. R. & Sabeti, P. C. Detecting natural selection in genomic data. *Annual review of genetics* **47**, 97–120, https://doi.org/10.1146/annurev-genet-111212-133526 (2013).
12. Kosakovsky Pond, S. L., Poon, A. F. Y., Leigh Brown, A. J. & Frost, S. D. W. A maximum likelihood method for detecting directional evolution in protein sequences and its application to influenza A virus. *Mol. Biol. Evol.* **25**, 1809–1824, https://doi.org/10.1093/molbev/msn123 (2008).
13. Steinbrück, L. & McHardy, A. C. Allele dynamics plots for the study of evolutionary dynamics in viral populations. *Nucleic Acids Res.* **39**, e4–e4, https://doi.org/10.1093/nar/gkq909 (2011).
14. Neher, R. A. & Bedford, T. nextflu: real-time tracking of seasonal influenza virus evolution in humans. *Bioinformatics* **31**, 3546–3548, https://doi.org/10.1093/bioinformatics/btv381 (2015).
15. Luksza, M. & Lassig, M. A predictive fitness model for influenza. *Nature* **507**, 57–61, https://doi.org/10.1038/nature13087 (2014).
16. Yang, Z. & Bielawski, J. P. Statistical methods for detecting molecular adaptation. *Trends Ecol. Evol.* **15**, 496–503 (2000).
17. Yang, Z. & Nielsen, R. E. Synonymous and Nonsynonymous Substitution Rates Under Realistic Evolutionary Models. *Mol. Biol. Evol.* **17**, 32–43, https://doi.org/10.1093/oxfordjournals.molbev.a026236 (2000).
18. Nei, M. & Gojobori, T. Simple methods for estimating the numbers of synonymous and nonsynonymous nucleotide substitutions. *Mol Biol Evol* **3**, 418–426 (1986).
19. Nielsen, R. *et al*. Genomic scans for selective sweeps using SNP data. *Genome Res.* **15**, 1566–1575, https://doi.org/10.1101/gr.4252305 (2005).
20. Kryazhimskiy, S. & Plotkin, J. B. The population genetics of dN/dS. *PLoS Genet.* **4**, e1000304–e1000304, https://doi.org/10.1371/journal.pgen.1000304 (2008).
21. Bhatt, S., Holmes, E. C. & Pybus, O. G. The genomic Rate of Molecular Adaptation of the Human Influenza A Virus. *Mol. Biol. Evol.*, 1–9, https://doi.org/10.1093/molbev/msr044 (2011).
22. Kim, Y. & Nielsen, R. Linkage Disequilibrium as a Signature of Selective Sweeps. *Genetics* **167**, 1513–1524, https://doi.org/10.1534/genetics.103.025387 (2004).
23. Wright, S. Evolution in Mendelian Populations. *Genetics* **16**, 97–159 (1931).
24. Fisher, R. A. On the dominance ratio. *Proceedings of the Royal Society of Edinburgh* **42**, 321–341 (1922).
25. Charlesworth, B. Effective population size and patterns of molecular evolution and variation. *Nat. Rev. Genet.* **10**, 195–205 (2009).
26. Wright, S. Inbreeding and Homozygosis. *Proc. Natl. Acad. Sci. USA* **19**, 411–420 (1933).
27. Wright, S. Size of population and breeding structure in relation to evolution. *Science* **87**, 430–431, doi:citeulike-article-id:13674781 (1938).
28. Hein, J., Schierup, M. H. & Wiuf, C. *Gene genealogies, variation and evolution: a primer in coalescent theory*. (Oxford University Press, USA, 2005).
29. Templeton, A. R. *Population genetics and microevolutionary theory*. (Wiley Online Library, 2006).
30. Fisher, R. A. On the Interpretation of $\chi 2$ from Contingency Tables, and the Calculation of P. *Journal of the Royal Statistical Society* **85**, 87–94, https://doi.org/10.2307/2340521 (1922).
31. Benjamini, Y. & Hochberg, Y. Controlling the False Discovery Rate: A Practical and Powerful Approach to Multiple Testing. *Journal of the Royal Statistical Society. Series B (Methodological)* **57**, 289–300 (1995).
32. Wille, M. *et al*. Frequency and patterns of reassortment in natural influenza A virus infection in a reservoir host. *Virology* **443**, 150–160, https://doi.org/10.1016/j.virol.2013.05.004 (2013).
33. Varich, N. L., Gitelman, A. K., Shilov, A. A., Smirnov, Y. A. & Kaverin, N. V. Deviation from the random distribution pattern of influenza A virus gene segments in reassortants produced under non-selective conditions. *Archives of virology* **153**, 1149–1154, https://doi.org/10.1007/s00705-008-0070-5 (2008).
34. Rambaut, A. *et al*. The genomic and epidemiological dynamics of human influenza A virus. *Nature* **453**, 615–619, https://doi.org/10.1038/nature06945 (2008).
35. Otte, A. *et al*. Evolution of 2009 H1N1 influenza viruses during the pandemic correlates with increased viral pathogenicity and transmissibility in the ferret model. *Scientific reports* **6**, 28583, https://doi.org/10.1038/srep28583 (2016).
36. Elderfield, R. A. *et al*. Accumulation of human-adapting mutations during circulation of A(H1N1)pdm09 influenza virus in humans in the United Kingdom. *J. Virol.* **88**, 13269–13283, https://doi.org/10.1128/jvi.01636-14 (2014).
37. Otte, A. *et al*. Adaptive mutations that occurred during 2009 H1N1 influenza virus pandemic circulation in humans enhance virulence in mice. *J Virol*. https://doi.org/10.1128/jvi.00665-15 (2015).
38. van Riel, D. *et al*. H5N1 Virus Attachment to Lower Respiratory Tract. *Science* **312**, 399, https://doi.org/10.1126/science.1125548 (2006).
39. Shinya, K. *et al*. Avian flu: influenza virus receptors in the human airway. *Nature* **440**, 435–436, https://doi.org/10.1038/440435a (2006).
40. Gabriel, G., Herwig, A. & Klenk, H. D. Interaction of polymerase subunit PB2 and NP with importin alpha1 is a determinant of host range of influenza A virus. *PLoS Pathog* **4**, e11, https://doi.org/10.1371/journal.ppat.0040011 (2008).
41. Sun, Y. *et al*. Naturally occurring mutations in the PA gene are key contributors to increased virulence of pandemic H1N1/09 influenza virus in mice. *J. Virol.* **88**, 4600–4604, https://doi.org/10.1128/jvi.03158-13 (2014).
42. Takahashi, T., Song, J., Suzuki, T. & Kawaoka, Y. Mutations in NA that induced low pH-stability and enhanced the replication of pandemic (H1N1) 2009 influenza A virus at an early stage of the pandemic. *PLoS One* **8**, e64439, https://doi.org/10.1371/journal.pone.0064439 (2013).
43. Abed, Y., Baz, M. & Boivin, G. Impact of neuraminidase mutations conferring influenza resistance to neuraminidase inhibitors in the N1 and N2 genetic backgrounds. *Antiviral therapy* **11**, 971–976 (2006).
44. Colman, P. M., Hoyne, P. A. & Lawrence, M. C. Sequence and structure alignment of paramyxovirus hemagglutinin-neuraminidase with influenza virus neuraminidase. *J Virol* **67**, 2972–2980 (1993).
45. de Vries, R. P. *et al*. Evolution of the hemagglutinin protein of the new pandemic H1N1 influenza virus: maintaining optimal receptor binding by compensatory substitutions. *J. Virol.* **87**, 13868–13877, https://doi.org/10.1128/jvi.01955-13 (2013).
46. Gabriel, G. *et al*. The viral polymerase mediates adaptation of an avian influenza virus to a mammalian host. *Proc Natl Acad Sci USA* **102**, 18590–18595, https://doi.org/10.1073/pnas.0507415102 (2005).
47. Butler, J. *et al*. Estimating the fitness advantage conferred by permissive neuraminidase mutations in recent oseltamivir-resistant A(H1N1)pdm09 influenza viruses. *PLoS Pathog* **10**, e1004065, https://doi.org/10.1371/journal.ppat.1004065 (2014).
48. He, D. *et al*. Global Spatio-temporal Patterns of Influenza in the Post-pandemic Era. *Sci Rep* **5**, 11013, https://doi.org/10.1038/srep11013 (2015).

49. Gabriel, G. *et al*. Differential use of importin-alpha isoforms governs cell tropism and host adaptation of influenza virus. *Nature communications* **2**, 156, https://doi.org/10.1038/ncomms1158 (2011).
50. Bussey, K. A. *et al*. PA residues in the 2009 H1N1 pandemic influenza virus enhance avian influenza virus polymerase activity in mammalian cells. *J. Virol.* **85**, 7020–7028, https://doi.org/10.1128/jvi.00522-11 (2011).
51. Laursen, N. S. & Wilson, I. A. Broadly neutralizing antibodies against influenza viruses. *Antiviral Res.* **98**, 476–483, https://doi.org/10.1016/j.antiviral.2013.03.021 (2013).
52. Kratsch, C., Klingen, T. R., Mümken, L., Steinbrück, L. & McHardy, A. C. Determination of antigenicity-altering patches on the major surface protein of human influenza A/H3N2 viruses. *Virus Evolution* **2** (2016).
53. Koel, B. F. *et al*. Substitutions near the receptor binding site determine major antigenic change during influenza virus evolution. *Science* **342**, 976–979, https://doi.org/10.1126/science.1244730 (2013).
54. Lin, Y. P. *et al*. Evolution of the receptor binding properties of the influenza A(H3N2) hemagglutinin. *Proc. Natl. Acad. Sci. USA* **109**, 21474–21479, https://doi.org/10.1073/pnas.1218841110 (2012).
55. Li, Y. *et al*. Single hemagglutinin mutations that alter both antigenicity and receptor binding avidity influence influenza virus antigenic clustering. *Journal of virology* **87**, 9904–9910, https://doi.org/10.1128/JVI.01023-13 (2013).
56. Steinbruck, L., Klingen, T. R. & McHardy, A. C. Computational prediction of vaccine strains for human influenza A (H3N2) viruses. *Journal of virology* **88**, 12123–12132, https://doi.org/10.1128/JVI.01861-14 (2014).
57. Who. Recommended composition of influenza virus vaccines for use in the 2015-2016 northern hemisphere influenza season. *Releve epidemiologique hebdomadaire/Section d'hygiene du Secretariat de la Societe des Nations=Weekly epidemiological record/Health Section of the Secretariat of the League of Nations* **90**, 97–108 (2015).
58. Who. Recommended composition of influenza virus vaccines for use in the 2005–2006 influenza season. *WHO Weekly Epidemiological Record* **80**, 66–71 (2005).
59. Ampofo, W. K. *et al*. Strengthening the influenza vaccine virus selection and development process: outcome of the 2nd WHO Informal Consultation for Improving Influenza Vaccine Virus Selection held at the Centre International de Conferences (CICG) Geneva, Switzerland, 7 to 9 December 2011. *Vaccine* **31**, 3209–3221, https://doi.org/10.1016/j.vaccine.2013.05.049 (2013).
60. Klingen, T. R., Reimering, S. & McHardy, A. C. hzi-bifo/SDplots: First release of SD plots data. *Zenodo*, https://doi.org/10.5281/zenodo.831631 (2017).
61. Reimering, S., Klingen, T. R. & McHardy, A. C. hzi-bifo/SDplots_VaccineUpdates: Prediction of influenza vaccine strains. *Zenodo*. https://doi.org/10.5281/zenodo.1026617 (2017).
62. Bao, Y. *et al*. The influenza virus resource at the National Center for Biotechnology Information. *J. Virol.* **82**, 596–601, https://doi.org/10.1128/JVI.02005-07 (2008).
63. Shu, Y. & McCauley, J. GISAID: Global initiative on sharing all influenza data – from vision to reality. *Eurosurveillance* **22**, 30494, https://doi.org/10.2807/1560-7917.ES.2017.22.13.30494 (2017).
64. Hay, A. J. *et al*. Interim Report September 2009. (WHO Collaborating Centre for Reference and Research on Influenza, National Institute for Medical Research, London, 2009).
65. Burke, D. F. & Smith, D. J. A Recommended Numbering Scheme for Influenza A HA Subtypes. *PLoS ONE* **9**, e112302, https://doi.org/10.1371/journal.pone.0112302 (2014).
66. Edgar, R. C. MUSCLE: multiple sequence alignment with high accuracy and high throughput. *Nucleic Acids Res.* **32**, 1792–1797, https://doi.org/10.1093/nar/gkh340 (2004).
67. Capella-Gutierrez, S., Silla-Martinez, J. M. & Gabaldon, T. trimAl: a tool for automated alignment trimming in large-scale phylogenetic analyses. *Bioinformatics* **25**, 1972–1973, https://doi.org/10.1093/bioinformatics/btp348 (2009).
68. Price, M. N., Dehal, P. S. & Arkin, A. P. FastTree 2–approximately maximum-likelihood trees for large alignments. *PLoS One* **5**, e9490, https://doi.org/10.1371/journal.pone.0009490 (2010).
69. WHO. Recommended composition of influenza virus vaccines for use in 2000. *WHO Weekly Epidemiological Record* 74, (321–328 (1999).
70. Fitch, W. M. Toward defining the course of evolution: minimum change for a specific tree topology. *Systematic Zoology* **20**, 406–416 (1971).
71. Sali, A. & Blundell, T. L. Comparative protein modelling by satisfaction of spatial restraints. *J Mol Biol* **234**, 779–815, https://doi.org/10.1006/jmbi.1993.1626 (1993).
72. Webb, B. & Sali, A. Comparative Protein Structure Modeling Using MODELLER. *Current protocols in bioinformatics* **47**, 5.6.1–32, https://doi.org/10.1002/0471250953.bi0506s47 (2014).
73. Kelley, L. A., Mezulis, S., Yates, C. M., Wass, M. N. & Sternberg, M. *J. The Phyre2 web portal for protein modeling, prediction and analysis.* **10**, 845–858, https://doi.org/10.1038/nprot.2015.053 (2015).
74. Reich, S. *et al*. Structural insight into cap-snatching and RNA synthesis by influenza polymerase. *Nature* **516**, 361–366, https://doi.org/10.1038/nature14009 (2014).
75. Winn, M. D. *et al*. Overview of the CCP4 suite and current developments. *Acta Crystallogr D Biol Crystallogr* **67**, 235–242, https://doi.org/10.1107/S0907444910045749 (2011).
76. Lee, B. & Richards, F. M. The interpretation of protein structures: estimation of static accessibility. *J Mol Biol* **55**, 379–400 (1971).
77. Chothia, C. The nature of the accessible and buried surfaces in proteins. *J. Mol. Biol.* **105**, 1–12 (1976).
78. Tien, M. Z., Meyer, A. G., Sydykova, D. K., Spielman, S. J. & Wilke, C. O. Maximum allowed solvent accessibilites of residues in proteins. *PLoS One* **8**, e80635, https://doi.org/10.1371/journal.pone.0080635 (2013).
79. WHO. Recommended composition of influenza virus vaccines for use in the 2004 influenza season. *WHO Weeky Epidemiological Record* **78**, 375–379 (2003).
80. WHO. Recommended composition of influenza virus vaccines for use in the 2005 influenza season. *WHO Weeky Epidemiological Record* **79**, 369–376 (2004).
81. WHO. Recommended composition of influenza virus vaccines for use in the 2005–2006 influenza season. *WHO Weeky Epidemiological Record* **80**, 65–76 (2005).
82. WHO. Recommended composition of influenza virus vaccines for use in the 2006–2007 influenza season. *WHO Weeky Epidemiological Record* **81**, 81–88 (2006).
83. WHO. Recommended composition of influenza virus vaccines for use in the 2008 influenza season. *WHO Weeky Epidemiological Record* **82**, 345–356 (2007).
84. WHO. Recommended composition of influenza virus vaccines for use in the 2012–2013 northern hemisphere influenza season. *WHO Weeky Epidemiological Record* **87**, 81–96 (2012).
85. WHO. Recommended composition of influenza virus vaccines for use in the 2013–2014 northern hemisphere influenza season. *WHO Weeky Epidemiological Record* **88**, 101–116 (2013).
86. WHO. Recommended composition of influenza virus vaccines for use in the 2015 southern hemisphere influenza season. *WHO Weeky Epidemiological Record* **89**, 441–456 (2014).
87. WHO. Recommended composition of influenza virus vaccines for use in the 2016 southern hemisphere influenza season. *WHO Weeky Epidemiological Record* **90**, 545–560 (2015).
88. WHO. Recommended composition of influenza virus vaccines for use in the 2011–2012 northern hemisphere influenza season. *WHO Weekly Epidemiological Record* **86**, 81–91 (2011).

89. WHO. Recommended viruses for influenza vaccines for use in the 2011 influenza season (southern hemisphere). *WHO Weeky Epidemiological Record* **85**, 402–412 (2010).
90. WHO. Recommended composition of influenza virus vaccines for use in the 2014 southern hemisphere influenza season. *WHO Weekly Epidemiological Record* **88**, 437–448 (2013).
91. Who. Recommended composition of influenza virus vaccines for use in the 2014-2015 northern hemisphere influenza season. *WHO Weekly Epidemiological Record* **89**, 93–104 (2014).

Acknowledgements

This work was supported by the Helmholtz Centre for Infection research. The Heinrich Pette Institute, Leibniz Institute for Experimental Virology, is supported by the Free and Hanseatic City of Hamburg and the Federal Ministry of Health.

Author Contributions

A.C.M. conceived the study. A.C.M. and T.R.K. planned and coordinated the study. A.C.M., S.R., T.R.K. and F.K. designed the methodology. T.R.K., S.R., J.L. and K.M. maintained the data, implemented the software and created results. A.C.M., S.R., J.L., T.R.K., G.G. and T.K. analyzed the results. T.R.K., S.R., J.L. and T.K. generated all visualizations. T.R.K., A.C.M. and S.R. wrote the original draft of this manuscript and all authors reviewed the manuscript.

Additional Information

Supplementary information accompanies this paper at https://doi.org/10.1038/s41598-017-18791-z.

Competing Interests: The authors declare that they have no competing interests.